RSC Advances

PAPER

View Article Online
View Journal | View Issue

Cite this: *RSC Adv.*, 2014, **4**, 52856

Investigation of the continuous flow sorption of heavy metals in a biomass-packed column: revisiting the Thomas design model for correlation of binary component systems†

Felycia E. Soetaredjo,* Alfin Kurniawan, L. K. Ong, Dimas R. Widagdyo and Suryadi Ismadji

Remediation of aquatic environments polluted by toxic heavy metals has become a focus of interest for many chemical and environmental engineers throughout the world. In the present study, rice straw was employed as a low-cost agricultural waste material for the removal of Cd(II) and Pb(II) ions from single and binary solutions. Isothermal biosorption experiments were conducted at 303.15 K using a column at various flow rates and bed heights. The breakthrough curves for single metal systems were fitted with the Thomas, Yoon-Nelson, bed-depth-service-time (BDST) and dose-response models. A new semi-empirical model based on the classical Thomas equation has been developed for simulation of the breakthrough curves for binary metal systems. This modified Thomas model, combined with sorption-inhibiting coefficients determining competitive sorption behavior, was found to represent the breakthrough data very adequately. The exhausted biosorbent bed was readily regenerated using an acid elution method involving a 0.05 mol l^{-1} HCl solution, and was reused for five consecutive sorption–regeneration cycles without significant loss of adsorption capacity. The used biosorbent also showed economic promise in the packed bed treatment of actual electroplating wastewater containing Cd(II) and Pb(II) ions.

Received 30th June 2014
Accepted 7th October 2014

DOI: 10.1039/c4ra06425a

www.rsc.org/advances

1. Introduction

With industrialization and the rapid growth of urban populations, the reserves and quality of surface waters are worsening due to excessive discharge of pollutants into the water bodies. Among the various types of water pollutants, heavy metals are the most life-threatening, due to their toxicity, carcinogenicity, resistance to biological degradation and long-term accumulation in the food chain.[1] Cadmium and lead are two heavy metals that have a number of desirable properties in a variety of industrial applications, including batteries, ammunition, electronic goods, metal finishing, and weighting and shielding applications. On the other hand, according to the priority list of hazardous substances issued by the US Agency for Toxic Substances and Disease Registry (ATSDR), lead and cadmium rank second and seventh, respectively, in terms of frequency of occurrence, toxicity level and potential for human exposure.[2] The removal of these heavy metals is therefore a matter of priority, not only in terms of environmental awareness but also for the protection of water resources.

Over the past decade, adsorption has become the method of choice for the purification of water and wastewater. The key advantages of adsorption methods include their high efficiency, cost-effectiveness and wide adaptability, and also the fact that they are environmentally acceptable and capable of generating effluents of high quality. The success of adsorption processes is, however, strongly dependent on selection of the adsorbent material and design of the separation unit. A wide range of materials have been evaluated for the adsorption of heavy metals, including microbial and seaweed biomass (living or dead), cellular products, activated carbons, sewage sludges, clays and clay-like minerals, hybrid materials and ordered mesoporous silica.[3–12] Among these, living or dead lignocellulosic biomass consisting of natural polymeric materials are promising alternatives to commercial adsorbents for the purification of metal-bearing effluents. These naturally occurring polymeric materials (*e.g.*, lignin, cellulose and hemicellulose) contain hydroxyl, carboxyl, phosphate and amino functional groups, all of which possess a specific ability to bind heavy metals.[13–15] With this in mind, rice straw residues, of which about 40 million tons per annum are generated in Indonesia alone, have been highlighted in the present study as a

Department of Chemical Engineering, Widya Mandala Surabaya Catholic University, Kalijudan 37, Surabaya 60114, East Java, Indonesia. E-mail: felyciae@yahoo.com; Fax: +62 31 389 1267; Tel: +62 31 389 1264

† Electronic supplementary information (ESI) available. See DOI: 10.1039/c4ra06425a

cheap source of biomass for the potential detoxification of heavy metals in aqueous solution.

In practical applications the adsorption operation is usually performed in a packed bed system, in which the effluent stream is passed through a column packed with a specific quantity of a suitable adsorbent. The design of a reliable packed bed adsorber requires the construction of a satisfactory modeling framework centered on establishing the shape of the breakthrough curve.[16] The characteristic shape of the breakthrough curve of an adsorption system depends strongly on the design data, such as flow rate, initial solute concentration and the dimensions of the adsorber. In recent years an increasing number of publications have appeared in the literature dealing with heavy metal adsorption in packed bed operations and breakthrough modeling.[17–21] However, studies related to single-solute adsorption are not entirely relevant to practical industrial wastewater treatment.

In practical wastewater treatment, two or more heavy metal species may coexist within the liquid system. Although a large number of studies have sought to establish mathematical models for simulating the breakthrough curves for binary or multicomponent systems, there remains a major challenge to construct a simple yet reliable model that has high accuracy and is computationally efficient. The building block of most breakthrough models for heavy metal sorption is based on rate-controlling mechanisms, typical examples being film diffusion, surface diffusion, pore diffusion, and combinations of these.[22–24] Most, if not all, of these mass transfer-based models have had only limited success due to the complexity of the modeling, which often requires advanced computer resources for resolution. On the other hand a semi-empirical modification of the well-established column model can be a more effective approach for constructing breakthrough curves which give a closer match to the experimental data. In line with this, the present study has aimed at providing a new column model based on the classical Thomas model, for simulation of the breakthrough curves of heavy metal (*e.g.*, Cd(II) and Pb(II)) sorption from binary mixtures. The effect of bed height and flow rate on the breakthrough characteristics for single and binary metal systems are discussed in detail. The practical application of rice straw in handling practical electroplating wastewater containing multiple metal ions has also been evaluated in terms of its adsorption performance and cycling efficiency, along with the possibility of transforming waste biosorbent into value-added products.

2. Experimental

2.1 Chemicals

Analytical grade cadmium nitrate tetrahydrate (98%) and lead nitrate (99%) were purchased from Sigma-Aldrich, Singapore, and used as supplied. Deionized water was employed throughout.

2.2 Preparation of biosorbent

Rice straw was collected from a rice field located in Blitar district, East Java. After collection the biomass was cut into pieces 1 × 1 cm and boiled in deionized water (solid–water ratio 1 : 10, in three successive 3 h stages) to remove colored materials and water-soluble compounds. The residual solid was filtered off under vacuum, and washed and dried in a forced convection oven at 80 °C for 48 h. The dried biomass was crushed using an IKA-Labortechnick grinder and sieved through US standard test sieve no. 50/60 (250–297 μm). The final product was stored in airtight plastic bags.

2.3 Packed-bed biosorption experiments

Cadmium and lead solutions were prepared by dissolving a specific amount of the nitrate salt in 1 l deionized water to give an initial concentration of 0.01 mmol l^{-1}. Laboratory-scale experiments were conducted in a glass column (i.d. 3 cm, length 40 cm) with a 0.2 cm layer of sintered discs (Por. 2 grade; United Scientific Industries) located at the top and bottom of the column to ensure a closely packed arrangement and prevent any loss of biosorbent. A programmable Masterflex L/S peristaltic pump (Cole-Parmer Instrument Co.) was used to maintain a constant flow rate. The experimental set-up is shown in ESI Fig. S1.†

A given quantity of biosorbent was tightly packed into the column to give a bed height of 10, 15 or 20 cm. Precautions were taken to avoid channeling and air pockets within the packed bed by soaking the column in deionized water for 2 h before the biosorption experiments. $Cd(NO_3)_2$ or $Pb(NO_3)_2$, or an equimolar mixture of the two, were continuously pumped to the top of the column (downflow mode) at a prescribed flow rate (10, 20 or 30 ml min^{-1}). A solution of 0.1 N HCl was used to adjust the pH of the metal effluents to between 5.5 and 6.0. The column experiments were conducted at room temperature over 8 h.

Preliminary investigation showed that the bed exhaustion time (t_e) was 8 h (t_e is the time at which solute concentration in the outlet stream reaches 95% of its initial concentration). Effluent samples from the exit of the column were collected periodically and analyzed for residual ion concentration. In the initial period of the experiments (2 h), 5 ml aliquots were collected every 15 min, and thereafter every half hour. Duplicate runs were conducted, and the data recorded are the mean of the two.

2.4 Determination of the residual concentration of metal ions

The residual concentrations of Cd(II) and Pb(II) ions in the outlet stream were analyzed on a Shimadzu AA-6200 atomic absorption flame emission spectrophotometer in an air-acetylene flame. The calibration curves for each metal were constructed by diluting standard solutions of $Cd(NO_3)_2$ and $Pb(NO_3)_2$ (Fisher Scientific) to obtain working solutions of varying concentrations (0.001 to 0.01 mmol l^{-1}). Maximum absorbance occurred at wavelength 217.0 nm for Pb(II) and 228.8 nm for Cd(II).

2.5 Characterization of biosorbent

The surface topography was determined on a JEOL JSM-6300F field emission *scanning electron microscope* (SEM) at an

accelerating voltage of 20 kV. An energy-dispersive X-ray (EDX) detection system was connected to the SEM for elemental analysis. Nitrogen adsorption isotherms were measured at 77 K using a Micromeritics ASAP 2010 automated sorptometer. The specific surface area was determined by the standard BET method applied to an adsorption branch in the relative pressure (p/p°) range 0.05–0.30. Total pore volume (V_T) was estimated from the quantity of nitrogen adsorbed at a relative pressure of 0.99. The determination of metal content was conducted on a PANalytical MiniPal QC energy-dispersive X-ray fluorescence (EDXRF) spectrometer. The surface functional groups were identified by infrared spectroscopy on a Shimadzu FTIR 8400S spectrophotometer.

2.6 Calculation

The amounts of metal ions adsorbed onto the packed biosorbent, also described as the dynamic uptake capacity (mmol g^{-1}), were calculated by eqn (1):

$$q_{bed} = M_r / m, \quad (1)$$

where m is the mass of packed biosorbent (g) and M_r represents the difference (mmol) between the influent metal load and that leaving the column. The parameter M_r can be determined by eqn (2):[25]

$$M_r = V_e C_0 - \sum \frac{(V_{n+1} - V_n)(C_{n+1} - C_n)}{2}, \quad (2)$$

where V_e is the throughput volume at column exhaustion (l), C_0 is the influent metal ion concentration (mmol l^{-1}), V_n is the throughput volume at the nth reading (l), V_{n+1} is the throughput volume at the $(n + 1)$th reading (l), C_n is the outlet metal ion concentration at the nth reading (mmol l^{-1}) and C_{n+1} is the outlet metal ion concentration at the $(n + 1)$th reading (mmol l^{-1}). The quantity of metal ions in the adsorbed phase at 1% breakthrough, q_b (mmol g^{-1}), is provided by the following relationship:[26]

$$q_b = \frac{Q \times t_{1\%} \times C_0}{1000 \times m}, \quad (3)$$

where $t_{1\%}$ is the column service time (min) when the outlet solute concentration is equivalent to 1% of the inlet concentration, Q is the flow rate (ml min^{-1}) and m is the mass of packed biosorbent (g).

3. Results and discussion

3.1 Characteristics of biosorbent

The electron micrographs illustrated in ESI Fig. S2(a)–(c)† show a rod-like structure, the biosorbent exhibiting the smooth uniform surface of native rice straw. The EDX spectrum shown in Fig. S2(d)† confirmed that silica and the alkali and alkaline earth metals (*e.g.*, Na, K and Ca) were the elemental constituents of native rice straw. The presence of cadmium and lead metals was also detected in the EDX spectrum of metal-loaded rice straw (Fig. S2(e)†), confirming that these metals were adsorbed on the surface of the biosorbent. SEM images also revealed that there had been no significant structural changes between native and metal-loaded rice straw. The BET specific surface area of native rice straw was relatively low (39.6 m^2 g^{-1}), with a total pore volume of 0.012 cm^3 g^{-1}, supporting the SEM information that the biosorbent had a non-porous structure.

The FTIR transmittance spectra (not shown) displayed a number of representative bands in native rice straw: stretching of H-bonded OH groups at 3418 cm^{-1}, symmetrical stretching of sp^3 C–H in CH_2 groups near 2850 cm^{-1}, stretching of C=O at 1758 cm^{-1}, assigned to carboxylic acids or aliphatic esters in lignin or hemicellulose, stretching of C=C in the aromatic rings of bound lignin at 1520 cm^{-1}, symmetrical sp^3 C–H bending at 1361 cm^{-1}, stretching of C–O corresponding to glycosidic linkages in cellulose and hemicellulose near 1100 cm^{-1}, out-of-plane sp^2 C–H bending at 675 cm^{-1} and Si–O–Si stretching in silica at 524 cm^{-1}. The binding of Cd(II) and Pb(II) on the surface of the biosorbent was confirmed by the absorption bands within the range 510–450 cm^{-1}, possibly arising from the stretching vibration of M–O bonding, where M refers to the divalent Cd(II) and Pb(II) cations. Specifically, the coordination modes of metal–carboxylate complexes can be categorized into unidentate coordination, bidentate chelating coordination or bidentate bridging coordination.[27] Taking into account the spectral information of $\Delta\nu(COO^-)_{complex}$ and the possibility of interaction between divalent metal atom and the second carboxylate oxygen of the COO^- moiety present in cellulose and hemicellulose structures, it can be suggested that Cd(II)– or Pb(II)–carboxylate complexes are coordinated in the bidentate bridging form. In this case, the bidentate carboxylate-binding mode is preferred to the monodentate mode, in order to minimize the steric repulsion between the incoming metal ions and the ligand moiety. Furthermore, the clear shift to lower wavenumbers in the position of the stretching peaks of hydroxyl and carboxylic groups near 3400 and 1750 cm^{-1} identifies the chemical interaction between metal species and these surface functional groups during the biosorption process.

3.2 Breakthrough analysis

3.2.1 Effect of bed height. The effect of biosorbent dosage on the dynamic uptake capacity was systematically examined by varying the bed height at constant flow and an initial metal ion concentration of 0.01 mmol l^{-1}. In the present study, the performance of a packed bed was determined over relative concentrations (C_t/C_0) between 0.01 (1% breakthrough) and 0.95 (95% breakthrough), derived from the safe water quality standards determined by local government.

In Fig. 1 it may be seen that the gradient of the breakthrough curves became less sharp with increasing bed height, representing a greater degree of bed uptake capacity. The mass transfer zone (MTZ) (*i.e.*, the active part of the packed bed where adsorption actually takes place) in the Cd(II)-loaded column was 7.67, 10.47 and 11.96 cm for 10, 15 and 20 cm bed height, respectively. A longer time to reach the break point was also accomplished using beds of increased height. The dynamic uptake capacity at 1% breakthrough for a 15 cm packing height was 6.20 × 10^{-4} mmol g^{-1} (0.070 mg g^{-1}) for Cd and 6.72 ×

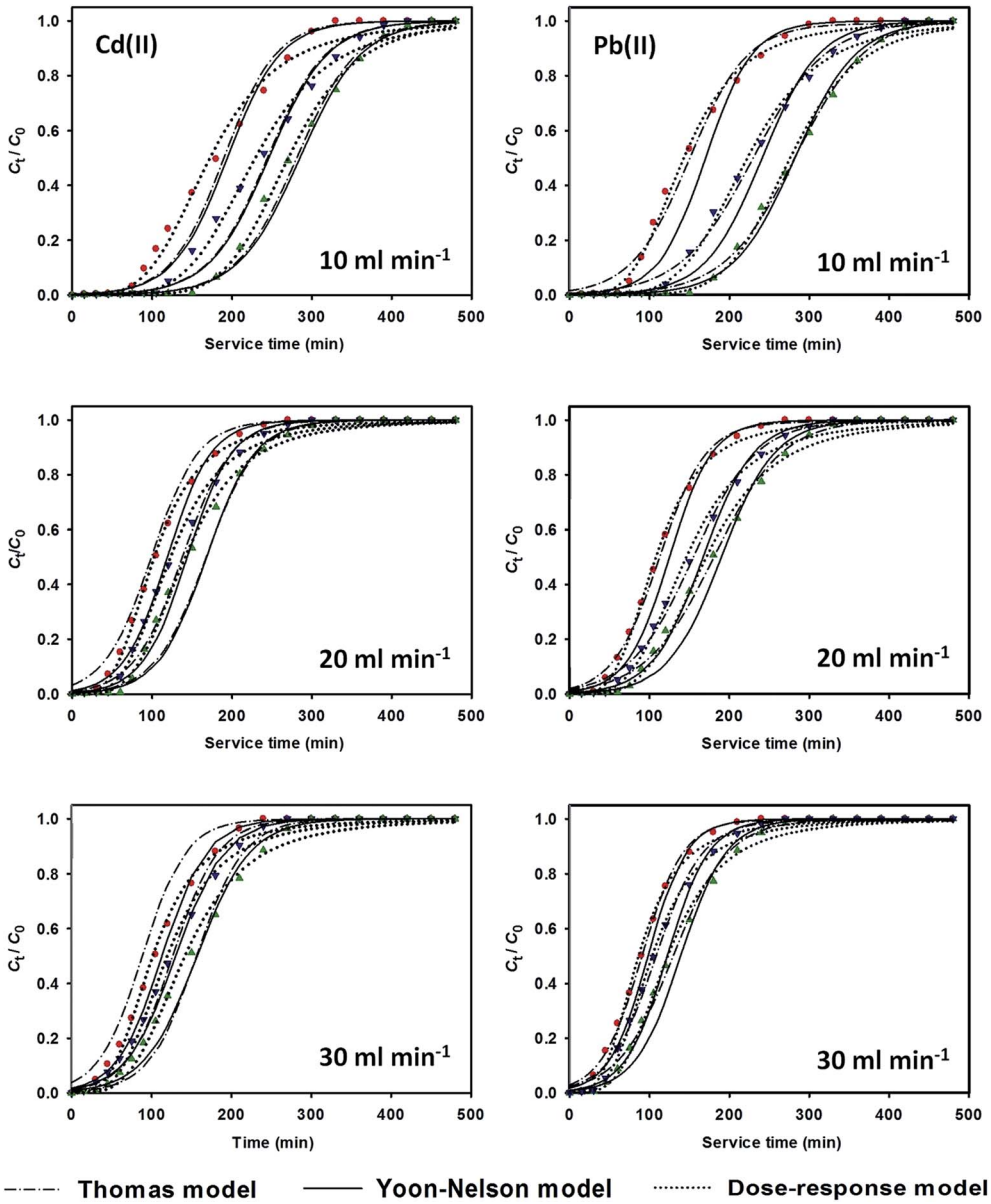

Fig. 1 Experimental breakthrough curves for single biosorption of Cd(II) and Pb(II) ions at various flow rates and bed heights (●10 cm – ▼15 cm – ▲20 cm) and the prediction results using the Thomas, Yoon-Nelson and dose-response models.

10^{-4} mmol g^{-1} (0.139 mg g^{-1}) for Pb; these values were increased to 6.74 × 10^{-4} mmol g^{-1} (0.076 mg g^{-1}) and 7.30 × 10^{-4} mmol g^{-1} (0.151 mg g^{-1}), respectively, for a 20 cm bed height by feeding the effluent at 10 ml min^{-1}.

This indicates that an increased bed height provided a greater depth of MTZ for the metal effluent to travel before reaching the exit, thus allowing a delayed breakthrough and an increase in the throughput volume of solution treated, ultimately extending the lifetime of the bed. With regard to bed exhaustion, beds with smaller heights become saturated more quickly due to a reduction in the number of superficial areas of the adsorbent, and consequently the active sites available for sorption.

3.2.2 Effect of solution flow rate. The breakthrough curves for single biosorption of Cd(II) and Pb(II) ions at various flow rates are shown in Fig. 1. An increase in steepness of the breakthrough curves was observed at higher flow rate, demonstrating an early breakthrough time and reduced bed exhaustion time. For a 20 cm bed height, as the solution flow rate was increased from 10 to 20 ml min^{-1} for Pb(II) sorption, the breakthrough time was reduced from 171 to 73 min and the exhaustion time from 395 to 300 min. These results can be explained by considering the limited contact time the metal effluent makes with the biosorbent bed, and also the limitation in the diffusion of metal ions from the liquid to the solid phase at higher flow rates, thus reducing the volume of solution being

treated and consequently decreasing the dynamic uptake capacity of the bed.

Furthermore, lower adsorption capacity at 1% breakthrough was obtained at higher flow rates. For example, by doubling the flow rate from 10 to 20 ml min^{-1}, the 20 cm breakthrough capacity of Cd(II) decreased from 6.74×10^{-4} mmol g^{-1} (0.076 mg g^{-1}) to 5.72×10^{-4} mmol g^{-1} (0.064 mg g^{-1}), and a further decrease to 4.48×10^{-4} mmol g^{-1} (0.050 mg g^{-1}) was noted as the flow rate increased to 30 ml min^{-1}.

3.3 Breakthrough modeling for the biosorption of single metals

The design and optimization of the breakthrough curve for a full-scale column adsorption system requires a simple modeling approach that can provide accurate scale-up column data. In the present study, the Thomas, Yoon-Nelson, BDST and dose-response empirical models were employed to analyze the breakthrough curves for single metal systems. The Thomas model is one of the most celebrated models used for describing column performance and the breakthrough curve, based on the Langmuir adsorption–desorption isotherms for the equilibrium and the second-order reversible reaction kinetics for the rate driving force without external and interparticle diffusion limitations.[28] The Thomas model has the following form:

$$\frac{C_t}{C_0} = \frac{1}{1 + \exp\left[K_{\mathrm{Th}}/Q\,(q_{\max} m - C_0 V_{\mathrm{T}})\right]}, \quad (4)$$

where K_{Th} is the Thomas rate constant (ml $mmol^{-1}$ min^{-1}), $q_{\max}$ is the intrinsic property of the adsorbent representing the maximum solid-phase concentration of solute (mmol g^{-1}), m is the mass of adsorbent (g), C_0 is the inlet concentration of solute (mmol l^{-1}), C_t is the exit concentration of solute at time t (mmol l^{-1}), Q is the solution flow rate (ml min^{-1}) and V_{T} is the cumulative throughput volume (l) of treated solution. The determination of Thomas parameters (K_{Th} and $q_{\max}$) was conducted by plotting $\ln(C_0/C_t - 1)$ *versus* t to give a straight line, with slope and intercept of $K_{\mathrm{Th}}C_0$ and $(K_{\mathrm{Th}}q_{\max}m)/Q$, respectively.

The second model applied for correlating the breakthrough curve was the Yoon-Nelson model. This model was developed by assuming that the rate of decrease in the probability of adsorption for each solute was proportional to the probability of its sorption and the breakthrough on the adsorbent.[29] The original and linearized forms of the Yoon-Nelson model for single component adsorption may be expressed by eqn (5) and (6), as follows:

$$\frac{C_t}{C_0} = \frac{\exp(K_{\mathrm{YN}}t - K_{\mathrm{YN}}\tau)}{1 + \exp(K_{\mathrm{YN}}t - K_{\mathrm{YN}}\tau)} \quad (5)$$

$$\ln\frac{C_t}{C_0 - C_t} = K_{\mathrm{YN}}t - K_{\mathrm{YN}}\tau, \quad (6)$$

where τ is the time (min) theoretically required to achieve 50% adsorbate breakthrough and K_{YN} is the Yoon-Nelson rate constant (min^{-1}).

The third model used for breakthrough curve analysis was the BDST model. The underlying assumption of the BDST model is that the adsorption rate is proportional both to the unused capacity of the adsorbent and to the remaining concentration of solute in the liquid phase, by neglecting the axial dispersion factor. The BDST model is regarded as a simple yet reliable model based on physical measurement of the adsorption capacity of the bed for different breakthrough values. The classical BDST model is expressed as follows:[30]

$$\ln\left(\frac{C_0}{C_{\mathrm{b}}} - 1\right) = \ln(\exp(K_{\mathrm{a}}N_0Z/u) - 1) - K_{\mathrm{a}}C_0t, \quad (7)$$

where C_{b} is the desirable breakthrough concentration (mmol l^{-1}), Z is the bed height (cm), N_0 is the volumetric sorption capacity of the bed (mmol l^{-1}), K_{a} is the adsorption rate constant (l $mmol^{-1}$ min^{-1}), and u is the linear velocity obtained by dividing the solution flow rate by the cross-sectional area of the bed (cm min^{-1}).

Eqn (7) has been further modified by Hutchins[31] to estimate the bed height required for a given service time at breakthrough point:

$$t_{\mathrm{b}} = \frac{N_0}{C_0u}Z - \frac{1}{K_{\mathrm{a}}C_0}\ln\left(\frac{C_0}{C_{\mathrm{b}}} - 1\right) \text{ when } \exp(K_{\mathrm{a}}N_0Z/u) \gg 1 \quad (8)$$

Solving eqn (8) for Z by substituting $t_{\mathrm{b}} = 0$:

$$Z_0 = \frac{u}{N_0K_{\mathrm{a}}}\ln\left(\frac{C_0}{C_{\mathrm{b}}} - 1\right), \quad (9)$$

where Z_0 is the minimum theoretical height required to give an exit concentration of C_{b} at zero time. Z_0 is often referred to as the critical bed height, and is clearly equal to the mass transfer zone length (MTZL). The dose-response model, first proposed by Viraraghavan and his group,[32] is an empirical model describing the biosorption of heavy metals during column operation. In practice, this model is better able to describe the kinetics of metal removal by the adsorption column than the Bohart–Adams or Thomas models, especially at lower and higher time periods on the breakthrough curve. The mathematical expression of the dose-response model is presented in eqn (10):

$$\frac{C_t}{C_0} = b_0 - \frac{b_0}{1 + \left(V_{\mathrm{T}}/b_1\right)^d}, \quad (10)$$

where the parameter b_0 is the expected response when saturation is reached, and is equal to unity as the time or throughput volume tends to infinity. The parameter b_1 indicates the throughput volume at which half of the maximum response occurs and m is a constant for the model. The dose-response model can be expressed differently by making $b_0 = 1$:

$$\frac{C_t}{C_0} = 1 - \frac{1}{1 + \left(V_{\mathrm{T}}C_0/qm\right)^d}, \text{ with } b_1 = qm/C_0 \quad (11)$$

The regression analysis of all column models against experimental breakthrough data was performed using Systat SigmaPlot 12.3.1 software, and the correlation model parameters obtained were used to construct the predicted breakthrough curves shown in Fig. 2. The accuracy of prediction of the models was further determined by computing the root mean square error (RMSE), defined as follows:

$$\mathrm{RMSE} = \sqrt{\frac{1}{N}\sum_{i=1}^{N}\left(y_{i,\mathrm{exp}} - y_{i,\mathrm{cal}}\right)^2}, \qquad (12)$$

where N is the number of experimental data, and $y_{i,\mathrm{exp}}$ and $y_{i,\mathrm{cal}}$ are the values obtained experimentally and by prediction, respectively.

As shown in Fig. 1, very good agreement is seen between the experimental and predicted column data by the Thomas, Yoon-Nelson and dose-response models. The coefficients of determination (R^2) for the three models are mostly greater than 0.94. The column correlation coefficients associated to each model are summarized in Tables 1 and 2.

The rate constants for the Thomas (K_{Th}) and Yoon-Nelson (K_{YN}) models decreased with increasing bed height and decreasing flow rate. The relationship between rate constant and bed height can be understood on the basis that the rate at which the MTZ traveled through the bed decreased with bed height, due to the increasing number of service areas treating the effluent. The higher rate constant suggested that a shorter bed would be sufficient to avoid breakthrough.[33]

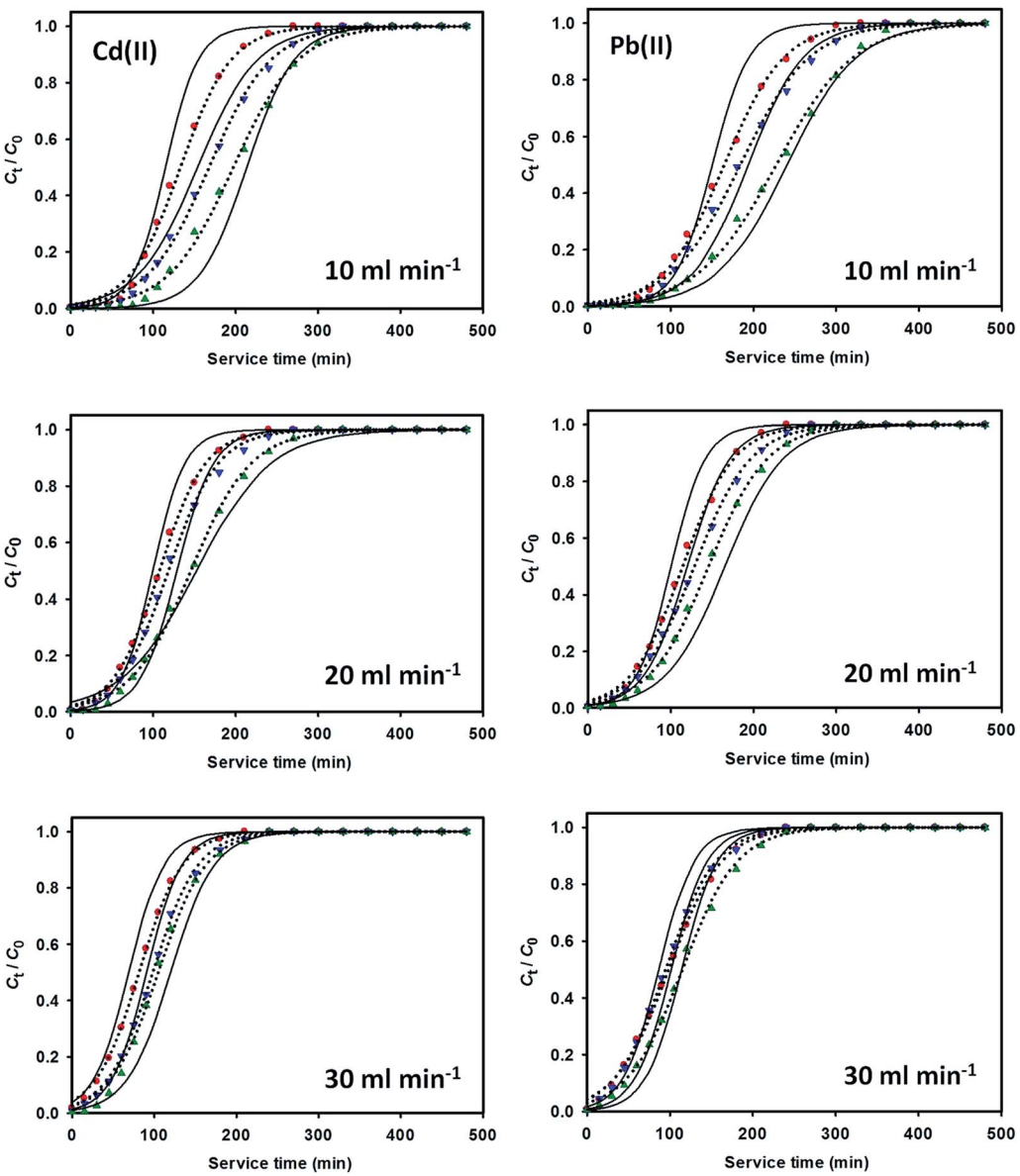

Fig. 2 Performance comparison between the original (solid lines) and modified Thomas model (dotted lines) in correlating the breakthrough curves for the binary sorption of Cd(II) and Pb(II) ions at various flow rates and bed heights (● 10 cm – ▼ 15 cm – ▲ 20 cm).

Table 1 The correlation parameters of the Thomas, Yoon-Nelson and dose-response models for single removal of Cd(II) and Pb(II) ions at varying bed heights (solution flow rate: 10 ml min^{-1} and influent metal concentration: 0.01 mmol l^{-1})

Thomas model						
Metal	Bed height (cm)	K_{Th} (l $mmol^{-1}$ min^{-1})	q_{max} (mmol g^{-1})	q_{bed}[a] (mmol g^{-1})	RMSE	R^2
Cadmium	10	3.06	1.62×10^{-3}	1.39×10^{-3}	0.056	0.948
	15	2.71	1.39×10^{-3}	1.18×10^{-3}	0.046	0.976
	20	2.64	1.20×10^{-3}	1.09×10^{-3}	0.029	0.981
Lead	10	3.25	1.79×10^{-3}	1.53×10^{-3}	0.089	0.940
	15	2.87	1.54×10^{-3}	1.29×10^{-3}	0.025	0.972
	20	2.79	1.32×10^{-3}	1.18×10^{-3}	0.016	0.984
Yoon-Nelson model						
Metal	Bed height (cm)	K_{YN} (min^{-1})	τ (min)	τ_{exp} (min)	RMSE	R^2
Cadmium	10	0.030	194	182	0.060	0.943
	15	0.027	246	236	0.048	0.967
	20	0.026	285	293	0.034	0.982
Lead	10	0.034	170	180	0.079	0.949
	15	0.028	241	238	0.051	0.960
	20	0.026	282	271	0.023	0.977
Dose-response model						
Metal	Bed height (cm)	q (mmol g^{-1})	b_1 (ml)	d	RMSE	R^2
Cadmium	10	1.47×10^{-3}	1721.37	3.94	0.038	0.993
	15	1.30×10^{-3}	2284.10	4.86	0.031	0.995
	20	1.15×10^{-3}	2694.45	6.42	0.021	0.998
Lead	10	1.42×10^{-3}	1428.62	3.89	0.025	0.997
	15	1.27×10^{-3}	2231.39	4.89	0.024	0.996
	20	1.18×10^{-3}	2764.74	6.44	0.022	0.997

[a] Dynamic uptake capacity, determined by eqn (1).

The maximum bed adsorption capacity obtained from the Thomas model prediction ranged between 0.92×10^{-3} and 1.79×10^{-3} mmol g^{-1} within the experimental conditions. However, the prediction overestimated the q_{bed} values obtained from eqn (1) by between 10 and 21%. This conspicuous difference has also been observed in a number of other column studies.[34–36] The increase in adsorption rate constant with flow rate might be attributed to a decrease in the fluid-film mass transfer resistance, meaning that solute molecules could diffuse more easily from the liquid to the solid phase. The correlation of column data by the Yoon-Nelson model also indicated that the time required for adsorbing 50% of the initial concentration decreased with increasing flow rate and decreasing bed height. In addition, the estimate of the time required to reach 50% breakthrough was very close to the values obtained experimentally.

The breakthrough curves predicted by the dose-response model showed an excellent fit to the experimental data. The column parameters associated with this model (q, b_1 and d) confirmed the dependence of these parameters on flow rate and the height of packed biosorbent. With an increase in mass of biosorbent from 11.71 g (10 cm) to 23.43 g (20 cm), the values of parameter q decreased from 1.42×10^{-3} to 1.18×10^{-3} mmol g^{-1} for Pb(II). The adsorption capacity of Cd(II) at 50% break point increased from 1.15×10^{-3} to 1.82×10^{-3} mmol g^{-1} as the flow rate increased from 10 to 30 ml min^{-1}; a similar effect applied to Pb(II) sorption. The parameter b_1 associated with the volumetric throughput at 50% break point also increased with increasing bed height and flow rate. The values of q and b_1 were each in conformity with the experimental data. The model constant (d) increased with increase in bed height and decrease in flow rate, suggesting that parameter d of the dose-response model might be related to the design of the fixed bed column, with improved adsorption performance.

The relationship between bed height and breakthrough level can be studied by applying the BDST model to the column data. ESI Fig. S3† shows the specific trends in the BDST column parameters (N_0, K_a and Z_0) with variation in the breakthrough points. The dynamic bed capacity of Cd(II) gradually increased from 0.127 to 0.154 mmol l^{-1} within a 1–40% breakthrough range. Within a breakthrough range of 60–95%, the dynamic bed capacity decreased and then increased to its highest point, 0.160 mmol l^{-1}. A similar trend was observed in the sorption of Pb(II), in which there was a sharp increase in the value of N_0

Table 2 The correlation parameters of the Thomas, Yoon-Nelson and dose-response models for single removal of Cd(II) and Pb(II) ions at varying solution flow rates (bed height: 20 cm and influent metal concentration: 0.01 mmol l^{-1})

Thomas Model						
Metal	Flow rate (ml min^{-1})	K_{Th} (l $mmol^{-1}$ min^{-1})	q_{max} (mmol g^{-1})	q_{bed}[a] (mmol g^{-1})	RMSE	R^2
Cadmium	10	2.64	1.20×10^{-3}	1.09×10^{-3}	0.029	0.981
	20	3.15	1.03×10^{-3}	0.85×10^{-3}	0.022	0.958
	30	3.36	0.92×10^{-3}	0.79×10^{-3}	0.052	0.965
Lead	10	2.79	1.32×10^{-3}	1.18×10^{-3}	0.016	0.984
	20	3.24	1.22×10^{-3}	1.08×10^{-3}	0.024	0.941
	30	3.45	1.11×10^{-3}	0.96×10^{-3}	0.023	0.958
Yoon-Nelson model						
Metal	Flow rate (ml min^{-1})	K_{YN} (min^{-1})	τ (min)	τ_{exp} (min)	RMSE	R^2
Cadmium	10	0.026	285	293	0.034	0.982
	20	0.029	168	147	0.074	0.954
	30	0.033	157	142	0.041	0.968
Lead	10	0.026	282	271	0.023	0.977
	20	0.030	190	180	0.051	0.948
	30	0.035	139	128	0.051	0.939
Dose-response model						
Metal	Flow rate (ml min^{-1})	q (mmol g^{-1})	b_1 (ml)	d	RMSE	R^2
Cadmium	10	1.15×10^{-3}	2694.45	6.42	0.021	0.998
	20	1.21×10^{-3}	2835.03	3.89	0.022	0.998
	30	1.82×10^{-3}	4264.26	3.64	0.032	0.995
Lead	10	1.18×10^{-3}	2764.74	6.44	0.022	0.997
	20	1.46×10^{-3}	3420.78	4.03	0.030	0.995
	30	1.57×10^{-3}	3678.51	3.62	0.023	0.998

[a] Dynamic uptake capacity, determined by eqn (1).

between 1% and 40% breakthrough, followed by a slight increase over the breakthrough range 60–95%. At low breakthrough points, there are a large number of vacant adsorption sites on the biosorbent, allowing metal ion uptake to occur with limited or no resistance. The dynamic capacity at 95% breakthrough (saturation) was found to be 0.160 mmol l^{-1} (0.11 mg g^{-1}) for Cd(II) and 0.198 mmol l^{-1} (0.25 mg g^{-1}) for Pb(II). Meanwhile, a gradually diminishing rate of transfer of solute from bulk fluid to the solid phase (K_a) with increasing breakthrough level was noticed, and the value of K_a remained relatively constant between 60 and 95% breakthrough. This might be ascribed to the limited degree of metal ion uptake, since more adsorption sites were occupied and an increasing proportion of the packed bed became saturated as the volume of effluent flowing into the column increased. The effect of diffusional resistance might also contribute significantly at high-end breakthrough levels, leading to slower uptake of metal ions.

The critical bed heights calculated at various breakthrough points showed a trend similar to that of the adsorption rate constant. For breakthrough points beyond 50%, it was not possible to calculate the critical bed height, due to the negative value of the natural logarithmic expression in eqn (9). This has also been confirmed by other authors,[37–39] indicating that the BDST model may be used only for interpretation of the initial part of the breakthrough curve, up to 50% breakthrough.

At 50% breakthrough the natural logarithmic expression in eqn (8) is reduced to zero and the bed capacity is estimated to be 0.157 mmol l^{-1} (0.11 mg g^{-1}) for Cd(II) and 0.194 mmol l^{-1} (0.24 mg g^{-1}) for Pb(II). These values are considerably lower than those reported by Bhatia and his group[39] for cadmium and lead ions removal in a fixed-bed column by a macro-fungus. They obtained an estimated 50% breakthrough capacity per unit bed volume of 8.54 and 7.72 mmol l^{-1} for Cd(II) and Pb(II) ions, respectively.

The fruit body of the oyster mushroom (*Pleurotus platypus*) has been utilized for the fixed-bed column removal of Cd(II) from industrial wastewater by Vimala and co-workers.[40] A breakthrough capacity per unit bed volume of 21.51 mmol l^{-1} was obtained from the BDST model prediction. A low adsorption capacity of the biomass bed was expected, and was probably due to the initial metal concentration used in the column experiments. It is well known that adsorption is a concentration-driven surface phenomenon, and the dependence of dynamic bed capacity on the initial solute concentration is confirmed mathematically from the slope of the

linear BDST plot in eqn (8). We purposely used low influent metal concentrations (1.12 mg l^{-1} of Cd(II) and 2.07 mg l^{-1} of Pb(II)) to represent the actual range of heavy metal contamination present in local public water systems.

Other fixed bed column parameters (*e.g.*, linear velocity) and the characteristics of the packing adsorbent might also contribute to determining the bed uptake capacity. Table 3 summarizes a comparison of the adsorption performance of various biosorbent materials for the single removal of Cd(II) and Pb(II) ions in a fixed bed operation. The poor prediction of the BDST model beyond a 50% breakthrough point could be attributed to the complex mechanisms of the binding of metal ions by the biosorbent, which might involve two or more rate-limiting steps, including ion exchange, coordination, complexation, chelation, micro-precipitation, adsorption and surface adsorption–complexation. Interestingly, the curve shows an S-like pattern for the variation of critical bed height with breakthrough points (ESI Fig. S3†), confirming the interrelationship of critical bed height and axial flow of MTZ inside the bed column.

Based on an analysis of all the column models discussed above, it could be deduced that the Yoon-Nelson and dose-response models provided a satisfactory representation for the present column system with respect to statistical parameters (RMSE or R^2) and the theoretical justification of the model parameters. From the goodness-of-fit point of view, the Thomas, Yoon-Nelson and dose-response models were all in general acceptable. While the BDST model demonstrated a satisfying linear correlation between column service time and bed height, the failure of this model beyond 50% breakthrough was inevitable. Further weaknesses of the BDST model were, firstly, that it assumed the adsorption of single solute in the liquid phase system and, secondly, it was unable to address the important effect of changes in pH, ionic form of the adsorbent or solute concentration on the column performance.[37] Regarding the Thomas model, the prediction of column kinetic data fell reasonably within the measured range, although a fairly significant deviation tended to occur within the initial part of the breakthrough curves. Additionally, a packing height of 10 cm was considered as the optimum bed height, since an increase in packing height of 5 cm or 10 cm to this point was insignificant in terms of the percentage metal removal (Table 4).

3.4 Breakthrough modeling for biosorption of binary component metals

In the present study, the simultaneous biosorption of Cd(II) and Pb(II) ions onto packed rice straw was conducted at flow rates of 10, 20 and 30 ml min^{-1} and packing heights of 10, 15 and 20 cm. An equimolar binary mixture containing 0.01 mmol l^{-1} of Cd(II) and Pb(II) ions was used as the effluent model. The breakthrough curves for binary metal solutions were required in order to study the effect between the metal ions and to assess the adsorption selectivity for one metal in the presence of another in a continuous flow system. In this regard, a modified Thomas design model incorporating the sorption-inhibiting coefficients was for the first time proposed to simulate the breakthrough curves of binary metal systems.

The general view of binary and/or multicomponent systems is that the solute species compete with one another for the available adsorption sites on the solid surface. Such behavior affects the rate of sorption of each solute, and consequently its concentration in the adsorbed phase. Therefore, the effect of competitive adsorption should be incorporated in the design model, and for this purpose we have introduced two dimensionless parameters as follows:

$$I_{12} = \frac{\theta_2}{\theta_1 + \theta_2} \quad (13)$$

and

$$I_{21} = \frac{\theta_1}{\theta_1 + \theta_2}, \quad (14)$$

Table 3 Comparison of BDST model-predicted bed capacity of various biomass materials for the removal of Cd(II) and Pb(II) ions in fixed bed column operation

Biomass	Influent Concentration (mmol l^{-1})	Column parameters		Predicted bed capacity (mmol l^{-1})	Reference
		Flow rate (ml min^{-1})	Bed Height (cm)		
P-doped rice husk	0.05 – Pb(II)	20	10–30	2.51×10^{-3}	20
Wheat straw	0.89 – Cd(II)	1000	50–200	2.77	34
Allspice residue	0.07 – Pb(II)	20	15	11.75 – Pb(II)	38
Sunflower waste carbon calcium-alginate beads	0.09 – Cd(II)	1	10–30	0.07	39
Macro fungus (*Pycnoporus sanguineus*)	0.7 – Cd(II) 0.38 – Pb(II)	10	4–15	7.72 – Pb(II) 8.54 – Cd(II)	40
Macro fungus (*Pleurotus platypus*)	0.09 – Cd(II)	5	5–15	21.51	41
Filamentous green algae (*Spirogyra neglecta*)	0.24 – Pb(II)	5	1	0.88	42
Spent *Agaricus bisporus*	0.24 – Pb(II)	5	4	32.01	43
Palm oil boiler mill fly ash	0.18 – Cd(II)	5	1–2	75.80	44
Rice straw	0.01 – Cd(II) 0.01 – Pb(II)	10	10–20	0.157 – Cd(II) 0.194 – Pb(II)	This study

Table 4 The breakthrough parameters for single biosorption of Cd(II) and Pb(II) ions at various bed heights and flow rates

Metal	Bed height (cm)	Flow rate (ml min^{-1})	t_b[a] (min)	t_e[a] (min)	MTZ[c] (cm)	q_b[b] ($\times 10^{-4}$ mmol g^{-1})	V_e (ml)	% R[d]
Cadmium	10	10	68	292	7.67	5.81	2920	93.5
		20	27	210	8.71	4.61	4200	85.6
		30	15	205	9.27	3.84	6150	78.7
	15	10	109	361	10.47	6.20	3610	93.8
		20	48	240	12.00	5.46	4800	85.8
		30	25	233	13.39	4.27	6990	79.2
	20	10	158	393	11.96	6.74	3930	94.0
		20	67	272	15.07	5.72	5440	86.1
		30	35	267	17.38	4.48	8010	79.4
Lead	10	10	72	270	7.33	6.15	2700	95.4
		20	32	212	8.49	5.47	4240	87.6
		30	18	178	8.99	4.61	5340	81.2
	15	10	118	361	10.10	6.72	3610	95.7
		20	51	271	12.18	5.81	5420	87.8
		30	29	210	12.93	4.95	6300	81.5
	20	10	171	395	11.34	7.30	3950	96.1
		20	73	300	15.13	6.23	6000	88.2
		30	42	237	16.46	5.38	7110	82.0

[a] Experimentally determined from Fig. 1, t_b and t_e were considered at 1% and 95% break points, respectively. [b] The bed adsorption capacity at 1% breakthrough, determined by eqn (3). [c] Mass transfer zone is calculated by $Z = (1 - t_b/t_e)$ where Z is the bed height (cm). [d] Removal percentage was calculated by dividing M_r with the influent metal load (V_eC_0).

where θ_1 and θ_2 represent the amounts of metal ions adsorbed, I_{12} and I_{21} are the sorption-inhibiting coefficients of component 2 (Pb(II)) to component 1 (Cd(II)) and *vice versa*. θ_1 and θ_2 are each treated as fractional parameters which account for the coordination complexes of metal ions with surrounding anions on the surface at the point of saturation. By introducing parameters I_{12} and I_{21} into the original Thomas model for each adsorbed component a modified Thomas model was obtained, with the inclusion of competitive adsorption behavior:

$$\left(\frac{C_t}{C_0}\right)_1 = \frac{1}{1 + \exp\left[\frac{K_{Th,1}(1 - I_{12})}{Q}\left(q_{1,max}m - C_{0,1}V_T\right)\right]} \quad (15)$$

$$\left(\frac{C_t}{C_0}\right)_2 = \frac{1}{1 + \exp\left[\frac{K_{Th,2}(1 - I_{21})}{Q}\left(q_{2,max}m - C_{0,2}V_T\right)\right]}, \quad (16)$$

where $K_{Th,1}$ and $K_{Th,2}$ are the sorption rate constants of component 1 and component 2 obtained from a single solute system (l mmol^{-1} min^{-1}), and $q_{1,max}$ and $q_{2,max}$ are the maximum bed sorption capacity for component 1 and component 2 in the binary system (mmol g^{-1}). θ_1, θ_2, $q_{1,max}$ and $q_{2,max}$ are fitted parameters, whose values can be determined by linear or nonlinear regression methods. The underlying assumptions of the proposed model are: (i) that the adsorption equilibrium is nonlinear and is well represented by the Langmuir isotherm; (ii) that the rate driving force obeys second-order reversible reaction kinetics, (iii) there is no axial dispersion; and (iv) that the adsorption system operates isothermally under given conditions.

The solution of eqn (15) and (16) can readily be obtained by nonlinear regression curve fitting, using Systat SigmaPlot 12.3.1 software or the Microsoft Excel 'Solver' function. To start the computation the initial values of all the fitted parameters were randomly estimated, with the following constraints: $\theta_1 > 0$, $\theta_2 > 0$, $q_{1,max} > 0$, $q_{2,max} > 0$ and $\theta_1 + \theta_2 < 1$. The computation was conducted point by point until the tolerance and convergence tests were fulfilled. We considered that the total portion of metal ions adsorbed on the surface ($\theta_1 + \theta_2$) was less than unity, by considering the free-volume fraction (porosity) in a fixed bed in which adsorption did not take place. The bed porosity (ε) was determined using eqn (17):

$$\varepsilon = 1 - \left(\rho_b/\rho_s\right), \quad (17)$$

where ρ_b and ρ_s are the tapped bulk density of the packed bed (g ml^{-1}) and the density of solid particles (g ml^{-1}), respectively, experimentally determined using a density meter. The applications of eqn (15) and (16) in correlating the experimental breakthrough data for an equimolar binary mixture of Cd(II) and Pb(II) ions are shown in Fig. 2, and the values of the fitted and calculated model parameters are summarized in Table 5.

It has been shown in Fig. 2 that the modified Thomas model correlated well with the experimental breakthrough curves for binary system ($R^2 \sim 0.99$), but the graphical fit showed that the original Thomas model (solid lines) was generally inadequate for describing the binary adsorption breakthrough curves, and an amplifying confirmation was provided by the coefficient of determination ($0.5 < R^2 < 0.7$). The incorporation of the dimensionless parameters, θ_1 and θ_2, to account for the effect of competitive adsorption between two solutes was therefore helpful in improving the goodness-of-fit of the proposed model. The values of the calculated parameters ($K_{Th,1}$ and $K_{Th,2}$) confirmed the applicability of the proposed modified Thomas model, in which the adsorption rate constants for each solute in the binary system were lower than the corresponding values for

Table 5 The fitted and calculated parameters of the modified Thomas model for binary sorption of Cd(II) and Pb(II) ions at various bed heights and flow rates

		Experimental		Fitted parameters				Calculated parameters					
Bed height (cm)	Flow rate (ml min^{-1})	$q_{bed,1}$ (mmol g^{-1})	$q_{bed,2}$ (mmol g^{-1})	θ_1	θ_2	$q_{max,1/bin}$ (mmol g^{-1})	$q_{max,2/bin}$ (mmol g^{-1})	I_{12}	I_{21}	$K_{Th,1/bin}$ (l $mmol^{-1}$ min^{-1})	$K_{Th,2/bin}$ (l $mmol^{-1}$ min^{-1})	RMSE	R^2
10	10	1.24×10^{-3}	1.44×10^{-3}	0.35	0.42	1.41×10^{-3}	1.57×10^{-3}	0.55	0.45	1.38	1.79	0.024	0.987
	20	1.74×10^{-3}	1.96×10^{-3}	0.37	0.43	1.96×10^{-3}	2.13×10^{-3}	0.54	0.46	1.69	1.92	0.017	0.993
	30	2.06×10^{-3}	2.38×10^{-3}	0.40	0.45	2.33×10^{-3}	2.69×10^{-3}	0.53	0.47	1.86	2.08	0.019	0.995
15	10	0.95×10^{-3}	1.12×10^{-3}	0.36	0.42	1.08×10^{-3}	1.29×10^{-3}	0.54	0.46	1.25	1.55	0.021	0.989
	20	1.31×10^{-3}	1.53×10^{-3}	0.38	0.44	1.46×10^{-3}	1.75×10^{-3}	0.54	0.46	1.57	1.84	0.017	0.992
	30	1.49×10^{-3}	1.75×10^{-3}	0.40	0.45	1.62×10^{-3}	1.92×10^{-3}	0.53	0.47	1.74	1.94	0.017	0.995
20	10	8.74×10^{-4}	9.48×10^{-4}	0.36	0.42	9.71×10^{-4}	1.08×10^{-3}	0.54	0.46	1.21	1.51	0.020	0.984
	20	1.12×10^{-3}	1.34×10^{-3}	0.38	0.44	1.24×10^{-3}	1.44×10^{-3}	0.54	0.46	1.45	1.75	0.014	0.997
	30	1.35×10^{-3}	1.56×10^{-3}	0.41	0.46	1.48×10^{-3}	1.71×10^{-3}	0.53	0.47	1.58	1.83	0.022	0.991

the single system. The presence of competing solutes not only decreases the adsorption rate constant, but also the maximum solid phase concentration of each solute. The values of the fractional parameters, θ_1 and θ_2, obtained by non-linear regression analysis showed that higher amounts of Pb(II) were sorbed on the packed bed.

EDXRF was performed to analyze the heavy metal content in the packed bed and to examine the conformity between EDXRF measurement and its theoretical calculation. The results indicate an error of at most 18% between the EDXRF measurement and the theoretical calculation, indicating that θ_1 and θ_2 can be treated as fractional parameters representing the amount of solutes adsorbed, in addition to the empirical correction coefficients for improving the graphical fit. The maximum bed adsorption capacity of Cd(II) predicted by the modified Thomas model declined from 1.62×10^{-3} mmol g^{-1} (0.18 mg g^{-1}) to 1.41×10^{-3} mmol g^{-1} (0.16 mg g^{-1}) when Pb(II) was present in the effluent for the fixed bed experiment at a flow rate of 10 ml min^{-1} and 10 cm bed height. Under these conditions, the maximum adsorption capacity of Pb(II) in the binary system was 1.57×10^{-3} mmol g^{-1} (0.33 mg g^{-1}), compared to 1.79×10^{-3} mmol g^{-1} (0.37 mg g^{-1}) in the single system.

Regarding the fitted parameters, θ_1 and θ_2, it can be implied that Pb(II) ions were adsorbed in preference to Cd(II), which may be ascribed to the smaller hydrated ionic radius of Pb(II) (4.01 Å) than Cd(II) (4.26 Å). It has been noted that the greater the hydration of the ion, the farther it is from the adsorbing surface, and the weaker its adsorptive capability. A consistent link between the hydrated ionic radii of the metals and their dynamic adsorption capacity was confirmed in the present study. Furthermore, according to Pearson's hard and soft (Lewis) acids and bases concept,[45] the Cd(II) cation is a "soft" Lewis acid, whereas the Pb(II) cation is a borderline Lewis acid. The Pb(II) cation can therefore form stronger complexes than the Cd(II) cation with electronegative ligands that are "hard" Lewis bases, such as F^-, OH^- or RO^- (carboxylate oxygen).

Increasing the solution flow rate resulted in an increased level of metal complex on the surface, whereas an increase in bed height had a small or no effect. Interestingly, the calculated sorption-inhibiting coefficients of the two metal ions showed a weak dependence on variation in flow rate and bed height. According to the results obtained, it can now be suggested that on changing either the flow rate or the bed height, the extent of competition between the adsorbed components remains essentially unchanged. Our hypothetical conclusion is that the extent of competition between the two solutes is more dependent on their initial concentrations in the binary system. Accordingly, further systematic investigation in this direction will be necessary by conducting the sorption-column tests using mixtures of various solute compositions.

3.5 Desorption studies and solid waste management

Once the biosorbent bed has become saturated with the metal ions, it is necessary to recover the metal species to allow the bed to be reused, and hence reduce operating costs. Column regeneration studies were conducted over five cycles of adsorption–desorption using hydrochloric acid at three different concentrations (0.1, 0.3 and 0.5 N) as desorbent. The flow rate of the desorbent solution was maintained at 10 ml min^{-1} using a peristaltic pump in the up-flow mode. Samples from the upstream of the column were collected every 10 min for analysis. The breakthrough time (min), exhaustion time (min) and breakthrough capacity (mmol g^{-1}) were determined for each sorption–regeneration cycle, and the results are shown in Table 6. As shown in this table, a decreased breakthrough time and exhaustion time was observed as the sorption–regeneration cycles progressed. The regeneration efficiency (%) was calculated using eqn (18):

$$\text{Efficiency } (\%) = q_R/q_o \times 100, \quad (18)$$

where q_R is the adsorption capacity of the regenerated biosorbent bed at the nth cycle (mmol g^{-1}) and q_o is the original adsorption capacity of the biosorbent bed (mmol g^{-1}).

Fig. 3 shows a set of graphical information about the desorption profiles of cadmium and lead ions through a 10 cm packed bed. A 93% recovery of Cd(II) was achieved by placing the exhausted bed in contact with 0.1 N HCl solution for 50 min, corresponding to a throughput volume of 0.50 l. After 30 min, a

five-fold increase in the concentration of HCl solution resulted in an increase in desorption efficiency from 74.6 to 91.1%. On the other hand, 0.1 N HCl (0.60 l) gave almost complete desorption of Pb(II) ions (~98%), and the throughput volume was reduced to 0.50 l using 0.5 N HCl solution.

Desorption of metal ions from the biosorbent wall takes place through an equivalent exchange reaction in which one mole of divalent Cd(II) or Pb(II) ions is displaced by two moles of H^+ ions.[46] Thus, an increase in the concentration of H^+ ions in the desorbent solution leads to an enhanced exchange performance between H^+ ions and metal ions at the solid–solution interface.

The stability performance of the biosorbent bed for up to five successive sorption–regeneration cycles was evaluated and the results are presented in Fig. 3(b). Prior to further cycles of adsorption–desorption, the eluted bed was washed a number of times with deionized water, until the pH of the washing solution was in the range 5.0–6.0. The washing step is essential to remove excess H^+ ions deposited on the surface of the biosorbent. It was shown that the adsorption capacity of the bed was almost equal for the first two cycles, but then dropped progressively from the third cycle to the fifth. The desorption of Pb(II) was nearly 90–92%, and in excess of 94% of sorbed Cd(II) was desorbed in each successive cycle. The lower desorption efficiency of Pb(II) reflects once again the higher adsorption affinity of the biosorbent for this metal ion. Compared to the original bed sorption capacity, the values after the fifth cycle corresponded to 84.64% for Cd(II) and 79.50% for Pb(II), showing good adsorptive retention efficiency, even though the biosorbent bed had been reused several times. By the end of the fifth cycle, about 2.97 and 3.26 l of individual effluents containing Cd(II) or Pb(II) ions had effectively been treated to reach the permissible concentration prior to discharge. The loss of biosorption performance after the bed had been consecutively regenerated and reused was due mainly to the detrimental effect of desorbing solution.[47]

Continual contact between HCl solution and biosorbent bed not only resulted in the dislocation of sorbed metal ions, but led also a gradual deterioration in the biosorbent structure. The SEM image in Fig. 3(c) shows some visible changes on the biosorbent surface structure after multiple sorption–regeneration cycles, indicating the leaching effect of hydrochloric acid during desorption, which may be responsible for the reduced metal biosorption capacity of the regenerated bed. An additional plausible reason for the decrease in the bed adsorption capacity during further cycles of adsorption and desorption could be the incomplete desorption of metal ions.

The management of solid waste is an environmental concern which has to be taken into account, since the disposal of metal-laden adsorbent on the land can contaminate the soil and leach into groundwater. The conversion of waste adsorbent materials to high-value end-products is therefore of considerable interest for environmental sustainability. The adsorptive capacity of the regenerated bed was considerably reduced after the tenth cycle, when less than 10% of its original adsorption capacity was retained. Elemental analysis by an EDXRF technique showed that the biosorbent bed contained 0.15 mmol g^{-1} (1.69 wt%) of Cd(II) and 0.16 mmol g^{-1} (3.31 wt%) of Pb(II).

An effective treatment for the solid waste is to employ a two-step thermal activation process at 700 °C for 4 h under a nitrogen atmosphere, followed at 900 °C for 2 h in an oxidizing (air) environment, producing activated carbon of high surface area. The porous properties and structural morphology of the resultant activated carbon are given in ESI Table S1 and Fig. S4, respectively.† The cadmium oxide- and lead oxide-impregnated carbons are each high-value products and may be further applied in a composite electrode for the electrocatalytic sensing of gaseous, inorganic and organic analytes,[48] catalysis of various oxidation and reduction reactions of gases and/or liquid chemicals,[49] or sorption-based water purification.[50]

3.6 Scale-up treatment of actual electroplating wastewater

For the scale-up experiments, the height and internal diameter of the column were 100 and 8 cm, with a scale-up ratio of 2.50-fold and 2.67-fold, respectively, from a laboratory-scale glass column. The detailed data of the scale-up parameters are given in ESI Table S2.† Actual electroplating wastewater was collected from a metal coating and plating unit located at the Surabaya Industrial Estate, Rungkut, East Java. The

Table 6 The breakthrough parameters of the original and regenerated biosorbent bed after five sorption-regeneration cycles[a]

Metal	Cycle no.	t_b (min)	t_e (min)	q_b[b] (mg g^{-1})	q_e[b] (mg g^{-1})	Desorption (mg g^{-1})	Regeneration efficiency (%)
Cadmium	1	68	292	0.065	0.280	0.265	Original
	2	65	287	0.062	0.276	0.263	98.57
	3	60	275	0.058	0.264	0.251	94.29
	4	54	262	0.052	0.252	0.242	90.00
	5	50	247	0.048	0.237	0.227	84.64
Lead	1	72	270	0.127	0.478	0.439	Original
	2	70	262	0.124	0.464	0.420	97.07
	3	65	252	0.115	0.446	0.411	93.31
	4	62	240	0.110	0.425	0.389	88.91
	5	57	215	0.101	0.380	0.343	79.50

[a] Note: bed height: 10 cm and flow rate of the metal influent and desorbing solution (0.5 N HCl): 10 ml min^{-1}. [b] The bed adsorption capacity at 1% and 95% breakthrough were calculated using eqn (3).

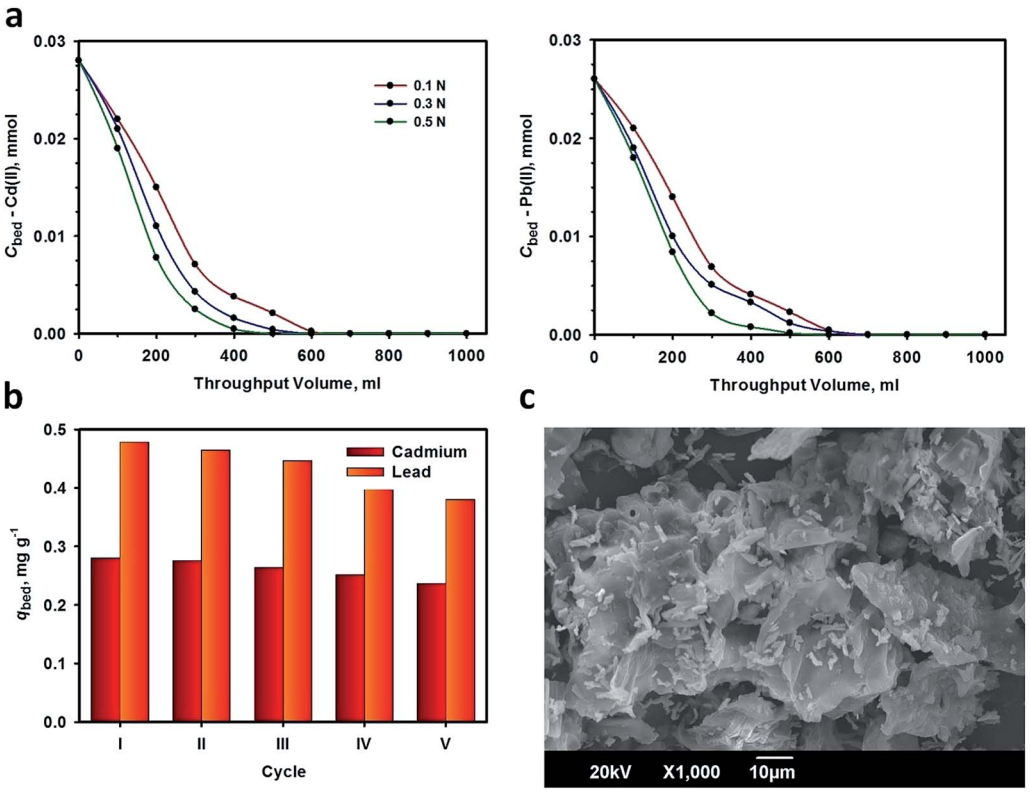

Fig. 3 (a) Desorption curves of Cd(II) and Pb(II) ions by HCl treatment at various concentrations; (b) the metal adsorptive retention after five sorption–regeneration cycles; and (c) SEM image shows the resulting morphology of biosorbent after desorption with 0.5 N HCl solution.

characteristics of the wastewater, including pH, total dissolved solids and chemical oxygen demand were analyzed using standard methods and the average concentrations of heavy metal species were measured using an atomic absorption spectrophotometer. The results are shown in ESI Table S3.† The pH adjustment of the wastewater was made by the appropriate addition of 0.1 N HCl.

The BDST laboratory-scale column parameters were used for prediction of the service time of the scaled-up column. The values obtained at a given flow rate (Q) and initial feed concentration (C_0) from laboratory-scale tests were used to calculate the BDST column parameters without further experimental determination, according to the relationship proposed by Cooney:[33]

$$\text{new slope} = \text{old slope}\left(\frac{Q_{\text{old}}}{Q_{\text{new}}}\right) \quad (19)$$

Eqn (19) was used to assess the change in dynamic adsorption capacity with flow rate. The intercept of the BDST equation related to adsorption rate constant remained unchanged with flow rate, and the new intercept value was thus equal to the old one. On the other hand, the slope and y-intercept of the BDST equation were both changed when the initial feed concentration was changed, and the new values can be calculated as follows:

$$\text{new slope} = \text{old slope}\left(\frac{C_{0,\text{old}}}{C_{0,\text{new}}}\right) \quad (20)$$

$$\text{new intercept} = \text{old intercept}\left(\frac{C_{0,\text{old}}}{C_{0,\text{new}}}\right) \times \left(\frac{\ln[(C_{0,\text{new}}/C_b) - 1]}{\ln[(C_{0,\text{old}}/C_b) - 1]}\right) \quad (21)$$

ESI Fig. S5a† shows the breakthrough curves for the individual heavy metals present in actual wastewater after biosorption through a 10 cm bed. It can be seen that the breakthrough curves for the biosorption of Cu(II), Cd(II) and Pb(II) ions each evolved in a similar manner, resembling the typical S-shape, while deformed breakthrough curves were observed for Cr(VI), Fe and Ni(II) ions. The deformed breakthrough curves for Cr(VI), Fe and Ni(II) ions might have been the result of the slow adsorption kinetics of these metal ions due to competition from other metal ions possessing greater specific binding affinity for certain surfaces.

The biosorbent bed also exhibited a lower adsorption capacity for Cd(II) (6.84×10^{-4} mmol g^{-1}) and Pb(II) (9.64×10^{-4} mmol g^{-1}) in the case of actual wastewater, compared to that in single and binary synthetic effluents. The loss of adsorption capacity may be attributed to the presence of multi-metal ions in the actual wastewater. ESI Fig. S5b† shows the percentage removal of each heavy metal, and it is clear that more than 50% of the total Cd(II) and Pb(II) ions in the real wastewater can still be removed using an appropriate amount of packed biosorbent.

The plots of the bed service time at breakthrough, obtained from experimental measurements and prediction by eqn (20) and (21) for Cd(II) and Pb(II) ions, are presented in ESI Fig. S5c.† For other heavy metals the figures are not presented, due to the unavailability of column data from laboratory-scale experiments. In Fig. S5c† it can be seen that for a 10 cm bed height, the predicted 1% breakthrough service time for Cd(II) and Pb(II) ions was 30 and 37 min, respectively. On the other hand, the predicted values are quite different from the experimental results, in which the 1% breakthrough service time was 18 min for Cd(II) and 28 min for Pb(II). This might suggest that the application of the BDST relationship proposed by Cooney for the purpose of column scale-up was limited to an adsorption system under comparable circumstances. Since real electroplating wastewater was used in the scale-up experiments, whereas synthetic aqueous solutions of Cd(II) and Pb(II) ions were used in the laboratory-scale tests, it is reasonable to expect some deviation between experimental and predicted breakthrough service time for such adsorption systems with different characteristics.

4. Conclusions

The use of a rice straw-packed column has demonstrated potential for removing toxic Cd(II) and Pb(II) ions from single and binary aqueous solutions. The breakthrough and saturation of the column is highly dependent on the flow rate and bed height. Increased service time of the column can be achieved by the use of greater bed height and a lower effluent flow rate. The Yoon-Nelson and dose-response models were successfully applied to describe the breakthrough curves for single metal systems obtained under varying bed heights and flow rates. Both empirical models provided a satisfactory correlation of experimental column data with the coefficient of determination (R^2) and theoretical justification of the model parameters. The binary breakthrough curves for binary metal system were reasonably well fitted by use of the modified Thomas model. Analysis of the binary breakthrough curves revealed that the extent of adsorption competition between the adsorbed solutes was not significantly affected by variations in flow rate and bed height. The packed biomass showed good reusability during multiple sorption–regeneration cycles without substantial loss of metal ion sorption capacity. Investigation of the adsorption performance on actual electroplating wastewater containing multiple metal ions demonstrated that the packed bed procedure can be applied in a highly effective manner, provided the pH of the wastewater is kept between 5.5 and 6. Spent rice straw can be considered a cheap and renewable biosorbent material for the effective removal of a number of metal ions in large-scale wastewater treatment.

Acknowledgements

A grant co-financed by the International Foundation for Science (IFS), Stockholm, Sweden and the Organization for the Prohibition of Chemical Weapons (OPCW) to Felycia Edi Soetaredjo, is gratefully acknowledged. We are also grateful to the National Taiwan University of Science and Technology (NTUST) for providing SEM and EDX facilities.

References

1 V. K. Gupta and I. Ali, *Sep. Purif. Technol.*, 2000, **18**, 131–140.
2 ATSDR, Priority List of Hazardous Substances, http://www.atsdr.cdc.gov/SPL/accessed 25 October, 2012.
3 E. Pehlivan, T. Altun and S. Parlayici, *Food Chem.*, 2012, **135**, 2229–2234.
4 I. Larraza, M. Lopez-Gonzalez, T. Corrales and G. Marcelo, *J. Colloid Interface Sci.*, 2012, **385**, 24–33.
5 J. Huang, M. Ye, Y. Qu, L. Chu, R. Chen, Q. He and D. Xu, *J. Colloid Interface Sci.*, 2012, **385**, 137–146.
6 M. Irani, M. Amjadi and M. A. Mousavian, *Chem. Eng. J.*, 2011, **178**, 317–323.
7 T. S. Anirudhan and S. S. Sreekumari, *J. Environ. Sci.*, 2011, **23**, 1989–1998.
8 L. Fan, C. Luo, Z. Lv, F. Lu and H. Qiu, *Colloids Surf., B*, 2011, **88**, 574–581.
9 S. Chowdhury and P. D. Saha, *Colloids Surf., B*, 2011, **88**, 697–705.
10 X. Zhang, H. Su, T. Tan and G. Xiao, *J. Hazard. Mater.*, 2011, **193**, 1–9.
11 Y. Tian, M. Wu, X. Lin, P. Huang and Y. Huang, *J. Hazard. Mater.*, 2011, **193**, 10–16.
12 L. Huang, C. Xiao and B. Chen, *J. Hazard. Mater.*, 2011, **192**, 832–836.
13 E. S. Abdel-Halim and S. S. Al-Deyab, *Carbohydr. Polym.*, 2012, **87**, 1863–1868.
14 X. Chen, K. F. Lam, S. F. Mak and K. L. Yeung, *J. Hazard. Mater.*, 2011, **186**, 902–910.
15 T. Y. Kim, S. K. Park, S. Y. Cho, H. B. Kim, Y. Kang, S. D. Kim and S. J. Kim, *Korean J. Chem. Eng.*, 2005, **22**, 91–98.
16 V. K. C. Lee, J. F. Porter and G. McKay, *Ind. Eng. Chem. Res.*, 2000, **39**, 2427–2433.
17 H. D. Doan, A. Lohi, V. B. H. Dang and T. Dang-Vu, *Process Saf. Environ. Prot.*, 2008, **86**, 259–267.
18 I. A. Aguayo-Villarreal, A. Bonilla-Petriciolet, V. Hernandez-Montoya, M. A. Montes-Moran and H. E. Reynel-Avila, *Chem. Eng. J.*, 2011, **167**, 67–76.
19 V. J. P. Vilar, C. M. S. Botelho and R. A. R. Boaventura, *Adsorption*, 2007, **13**, 587–601.
20 S. Mohan and G. G. Sreelakshmi, *J. Hazard. Mater.*, 2008, **153**, 75–82.
21 X. Luo, Z. Deng, X. Lin and C. Zhang, *J. Hazard. Mater.*, 2011, **187**, 182–189.
22 D. C. K. Ko, J. F. Porter and G. McKay, *Chem. Eng. Sci.*, 2005, **60**, 5472–5479.
23 C. W. Cheung, C. K. Chan, J. F. Porter and G. McKay, *Environ. Sci. Technol.*, 2001, **35**, 1511–1522.
24 B. Chen, C. W. Hui and G. McKay, *Water Res.*, 2001, **35**, 3345–3356.
25 P. A. Kumar and S. Chakraborty, *J. Hazard. Mater.*, 2009, **162**, 1086–1098.
26 D. K. C. Ko, J. F. Porter and G. McKay, *Water Res.*, 2001, **35**, 3876–3886.

27 K. Nakamoto, *Infrared and Raman Spectra of Inorganic and Coordination Compounds: Part B: Applications in Coordination, Organometallic, and Bioorganic Chemistry*, Wiley Interscience, New York, 6th edn, 2008.
28 H. C. Thomas, *J. Am. Chem. Soc.*, 1944, **66**, 1664–1666.
29 Y. H. Yoon and J. H. Nelson, *Am. Ind. Hyg. Assoc. J.*, 1984, **45**, 509–516.
30 G. S. Bohart and E. Q. Adams, *J. Am. Chem. Soc.*, 1920, **42**, 523–544.
31 R. A. Hutchins, *Chem. Eng. (N.Y.)*, 1973, **80**, 133–138.
32 G. Yan, T. Viraraghavan and M. Chen, *Adsorpt. Sci. Technol.*, 2001, **19**, 25–43.
33 D. O. Cooney, *Adsorption Design for Wastewater Treatment*, CRC Press, Boca Raton, 1998.
34 H. Muhamad, H. Doan and A. Lohi, *Chem. Eng. J.*, 2010, **158**, 369–377.
35 K. Vijayaraghavan, J. Jegan, K. Palanivelu and M. Velan, *Chemosphere*, 2005, **60**, 419–426.
36 G. Yan and T. Viraraghavan, *Bioresour. Technol.*, 2001, **78**, 243–249.
37 V. Sarin, T. S. Singh and K. K. Pant, *Bioresour. Technol.*, 2006, **97**, 1986–1993.
38 J. Cruz-Olivares, C. Perez-Alonso, C. Barrera-Diaz, F. Urena-Nunez, M. C. Chaparro-Mercado and B. Bilyeu, *Chem. Eng. J.*, 2013, **228**, 21–27.
39 M. Jain, V. K. Garg and K. Kadirvelu, *Bioresour. Technol.*, 2013, **129**, 242–248.
40 Z. Zulfadhly, M. D. Mashitah and S. Bhatia, *Environ. Pollut.*, 2001, **112**, 463–470.
41 R. Vimala, D. Charumathi and N. Das, *Desalination*, 2011, **275**, 291–296.
42 A. Singh, D. Kumar and J. P. Gaur, *Water Res.*, 2012, **46**, 779–788.
43 Y. Long, D. Lei, J. Ni, Z. Ren, C. Chen and H. Xu, *Bioresour. Technol.*, 2014, **152**, 457–463.
44 A. S. A. Aziz, L. A. Manaf, H. C. Man and N. S. Kumar, *Environ. Sci. Pollut. Res.*, 2014, **21**, 7996–8005.
45 R. G. Pearson, *J. Am. Chem. Soc.*, 1963, **85**, 3533–3539.
46 I. A. H. Schneider, J. Rubio and R. W. Smith, *Int. J. Miner. Process.*, 2001, **62**, 111–120.
47 B. Volesky, J. Weber and J. M. Park, *Water Res.*, 2003, **37**, 297–306.
48 B. Sljukic, C. E. Banks, A. Crossley and R. G. Compton, *Anal. Chim. Acta*, 2007, **587**, 240–246.
49 K. Otto, C. Lehman, L. Bartosiewicz and M. Shelef, *Carbon*, 1982, **20**, 243–251.
50 M. R. Yu, Y. Y. Chang and J. K. Yang, *Environ. Technol.*, 2012, **33**, 1553–1559.